Supplementary Information (SI) for Materials Chemistry Frontiers.
This journal is © the Partner Organisations 2026

Supplementary Information

Electrochemical Kinetics and Energy Storage Performance of 3D Hierarchical $CuFeS_2$@rGO Micro-flower Electrodes

Parul[a], Surjit Sahoo[b], Satyajit Ratha[c], Saroj Kumar Nayak[a*]

[a]*Indian Institute of Technology Bhubaneswar, Argul, Jatani, Khordha, Odisha-752050, India*

[b]*Centre for Interdisciplinary Research, SRM University-AP, Amaravati, Andhra Pradesh 522240, India*

[c]*Institute of Technical Education and Research, S'O'A Deemed to be University, Bhubaneswar, Odisha, India - 751030*

*Email address: nayaks@iitbbs.ac.in

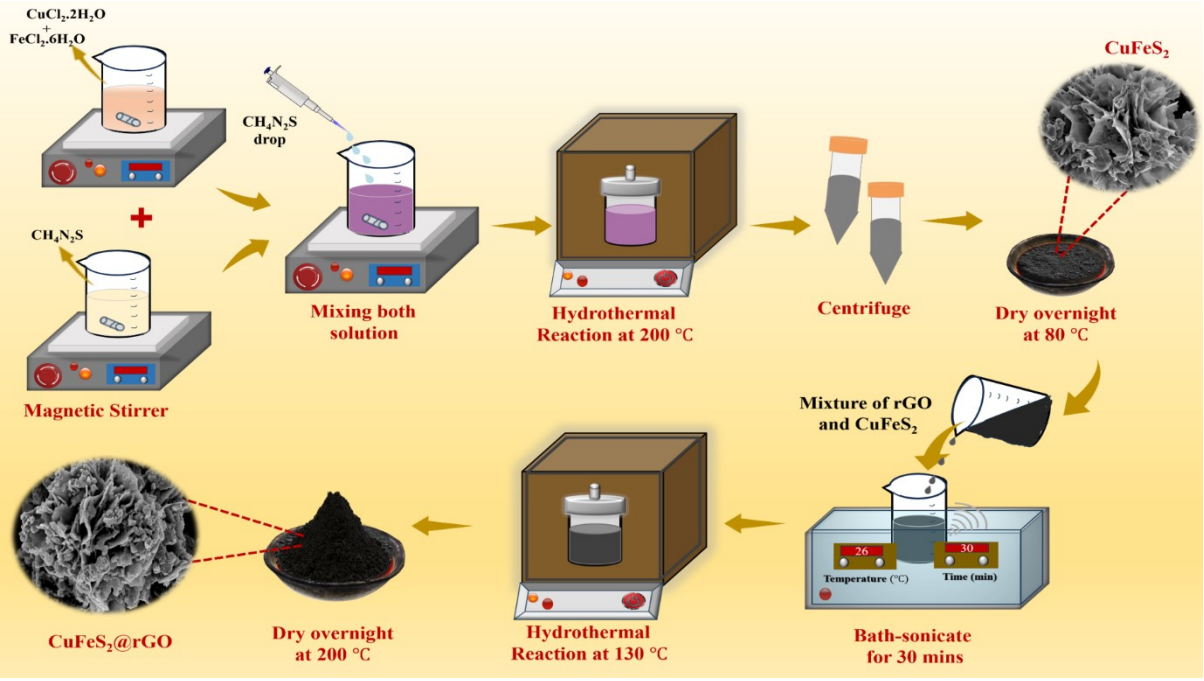

Figure S1 Schematic illustration of the preparation process for copper iron sulphide and its reduced graphene oxide composite.

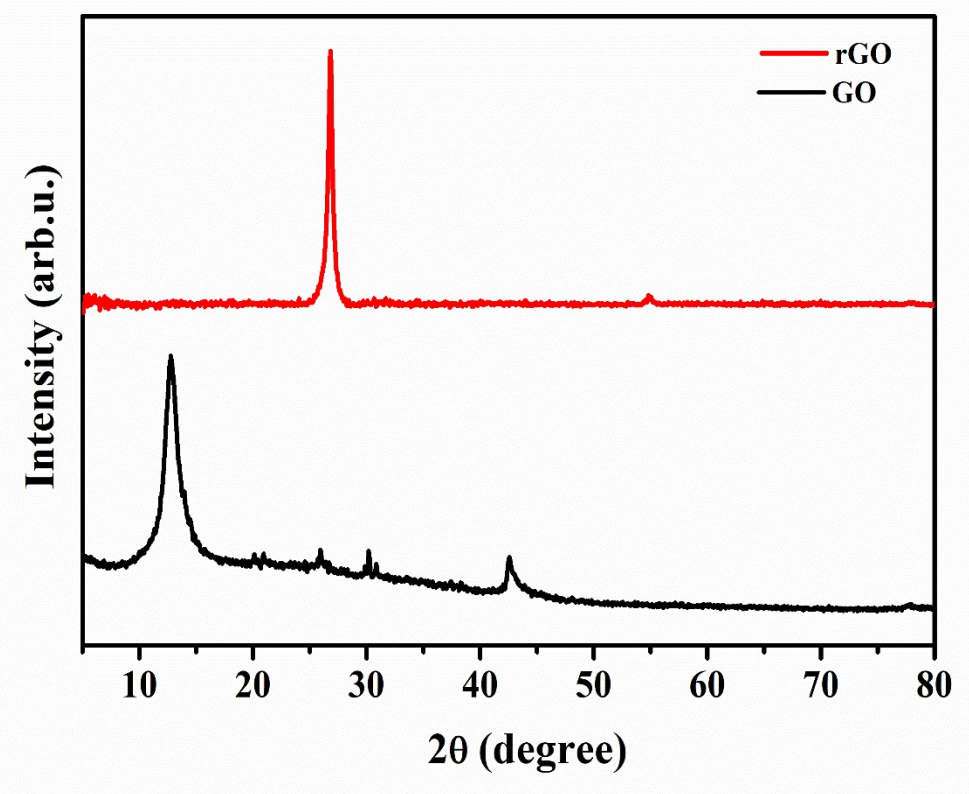

Figure S2 Comparison of Powder XRD for Graphene Oxide and Reduced Graphene Oxide.

1.1 Crystallographic information from XRD:

Furthermore, we calculated the d-spacing using Bragg's law (**equation 1**) to verify the lattice parameters a, b, and c.

$$n\lambda = 2d \sin\theta$$

or

$$d = \frac{n\lambda}{2sin\Theta} \quad \text{... (1)}$$

where d is the interplanar spacing (Å), n is 1 (diffraction order), θ is the peak position (in radians), and λ is 1.5406 Å. We have used **equation 2** for the tetragonal phase. ($a = b \neq c$), based on the tetragonal lattice relationship: [S19]

$$\frac{1}{d^2} = \frac{h^2 + k^2}{a^2} + \frac{l^2}{c^2} \quad \ldots (2)$$

This allowed us to calculate the lattice constant and d-spacing, which are all shown in the supplementary information (SI) in **Tables S1** and **S2**. The lattice parameters a and b were determined to be 5.2506 Å, and the lattice parameter c was calculated to be approximately 10.50 Å. This indicates that the calculated values of a, b, and c closely match the JCPDS file no. 00-035-0752 (standard value), indicating that the expected crystal structure was successfully formed.

The diffraction peak shows broadening, suggesting the nanoscale nature of the $CuFeS_2$ crystalline. **Equation 3**, also known as the Scherrer equation[S18], is used to calculate the crystalline size of $CuFeS_2$:

$$D = {}^{k\lambda}/_{\beta Cos\theta} \quad \ldots (3)$$

where k is a shape factor (constant) of 0.9, D represents the crystalline size, λ is the XRD wavelength (0.15 nm for CuKα radiation), β indicates the peak broadening at half maximum intensity, and θ is the Bragg angle or peak position. Using the Scherrer equation, the crystalline size has been determined to be 18.74 nm.

Table S1 Calculated d-spacing values at various peak positions.

Sr. no.	Peak position	Interplanar spacing	Miller indices
	2 θ (Å)	d (Å)	(hkl)
1.	29.44	3.03153	112 **(for c)**
2.	49.035	1.8564	220 **(for a = b)**
3.	57.97	1.5896	312
4.	58.63	1.57329	116
5.	79.47	1.2050	316

Table S2 Comparison of Actual and Calculated Lattice Parameters.

Sr. no.	Lattice parameters (Å)	Actual values (JCPDF file 01-035-0752)	Calculated values
1.	a	5.2893	5.2506
2.	b	5.2893	5.2506
3.	c	10.4230	10.5000

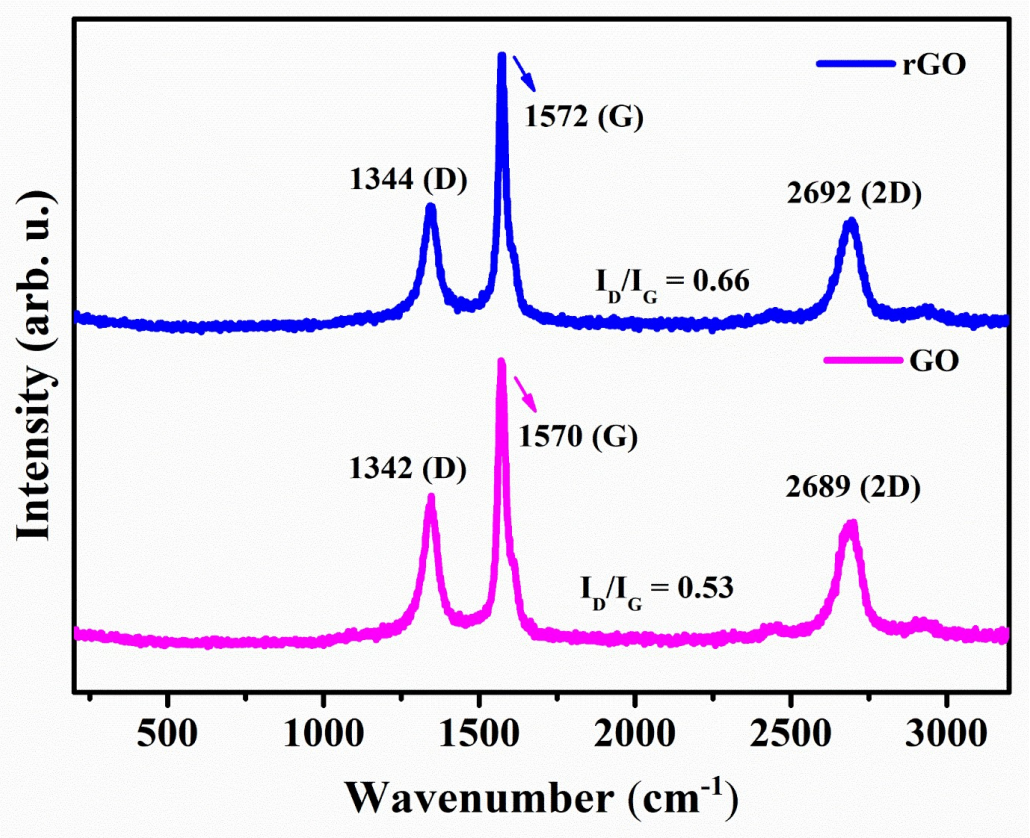

Figure S3 Raman Spectroscopy for Graphene Oxide and Reduced Graphene Oxide.

Table S3 Detailed **s**ummary of Raman study for GO, rGO, $CuFeS_2$, and $CuFeS_2$@rGO.

Sample name	Peak 1 (P1) cm^{-1}	Peak 2 (P2) cm^{-1}	Peak 3 (P3) cm^{-1}	Peak 3 (P4) cm^{-1}	D-band position in cm^{-1}	G-band position in cm^{-1}	2D-band position in cm^{-1}	I_D/I_G	L_a (nm)
GO	-	-	-	-	1344	1572	2692	0.53	36.3
rGO	-	-	-	-	1342	1570	2689	0.66	29.1
$CuFeS_2$	290	316.0	347	470	-	-	-	-	-
$CuFeS_2$@rGO	291	316.5	347	471	1347	1574	2698	0.75	25.6

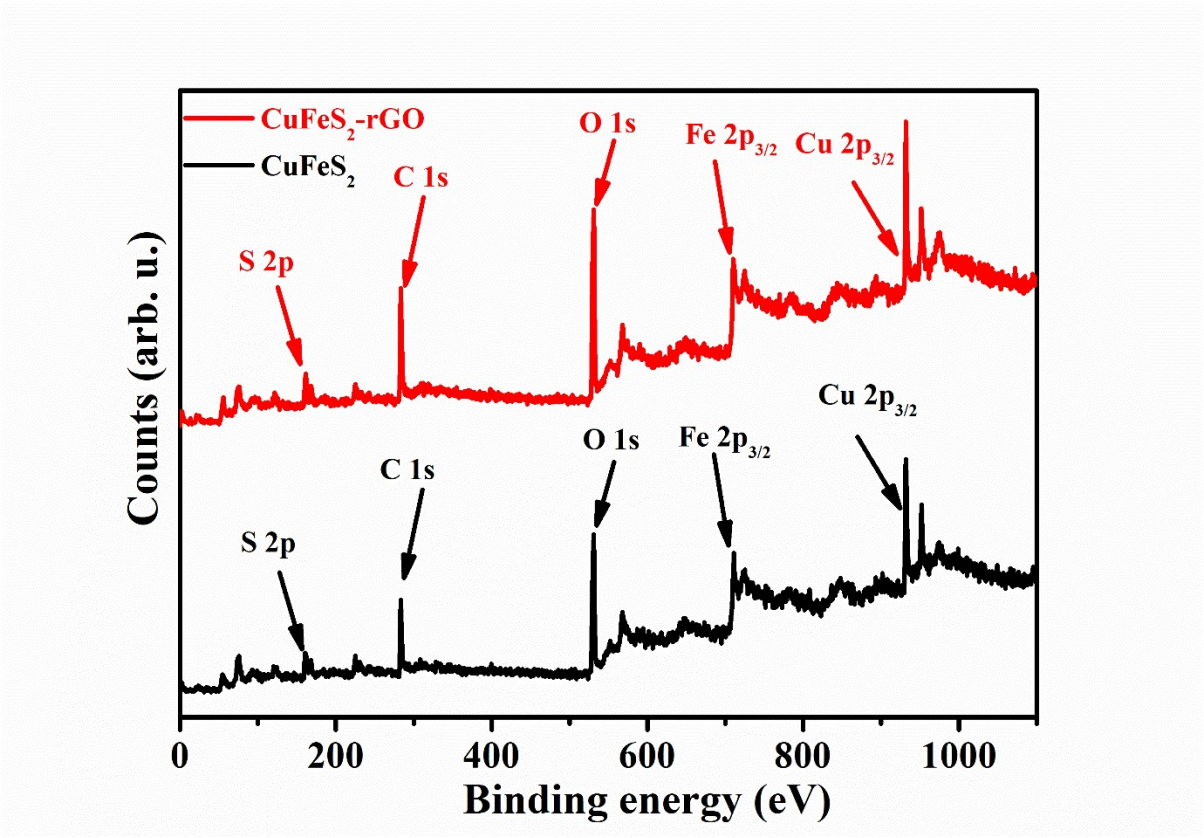

Figure S4 XPS survey spectra for bare $CuFeS_2$ and $CuFeS_2$@rGO composite.

Table S4 Physical properties of bare $CuFeS_2$ and $CuFeS_2$@rGO composite.

Sample name	Surface area (m^2/g)	Pore Diameter (nm)	Pore volume (CC/g)
$CuFeS_2$	6.297	16.24	0.0237
$CuFeS_2$@rGO	22.709	24.05	0.1256

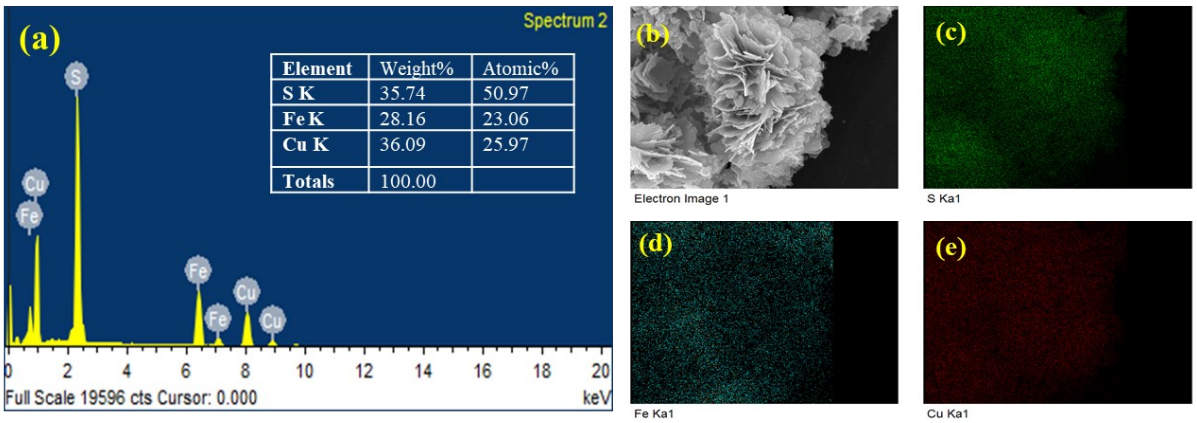

Figure S5 (a) The EDX spectrum of $CuFeS_2$, (b) FE-SEM micrograph for elemental mapping of $CuFeS_2$, (c) Sulphur, (d) Iron, (e) Copper.

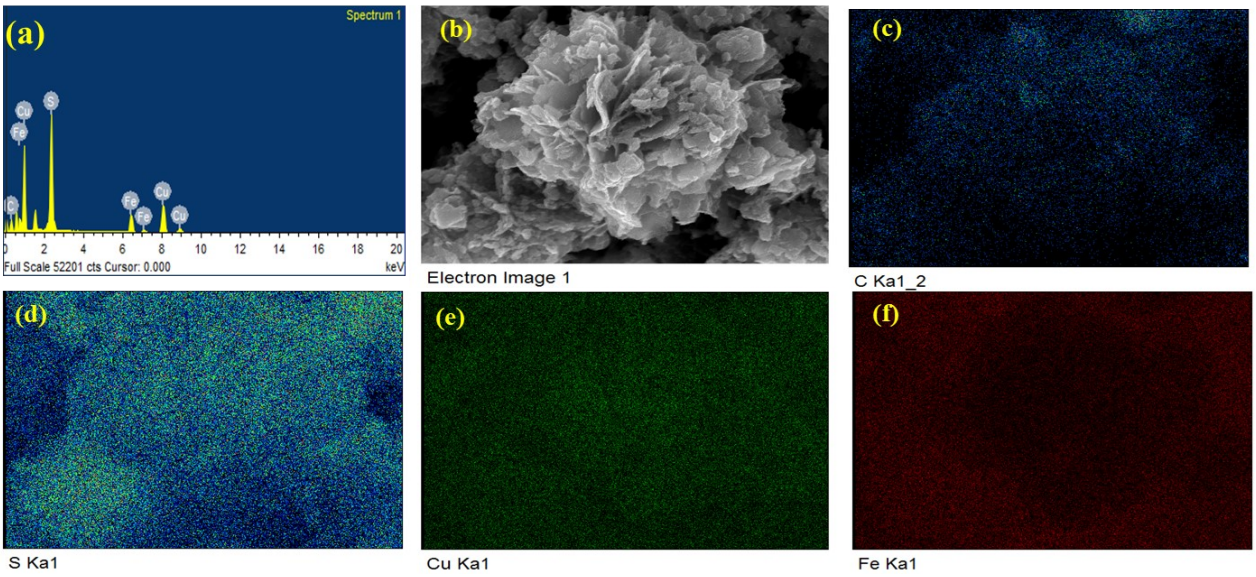

Figure S6 (a) The EDX spectrum of $CuFeS_2$@rGO, (b) FE-SEM micrograph for elemental mapping of $CuFeS_2$@rGO, (c) carbon, (d) sulphur, (e) iron, (f) copper.

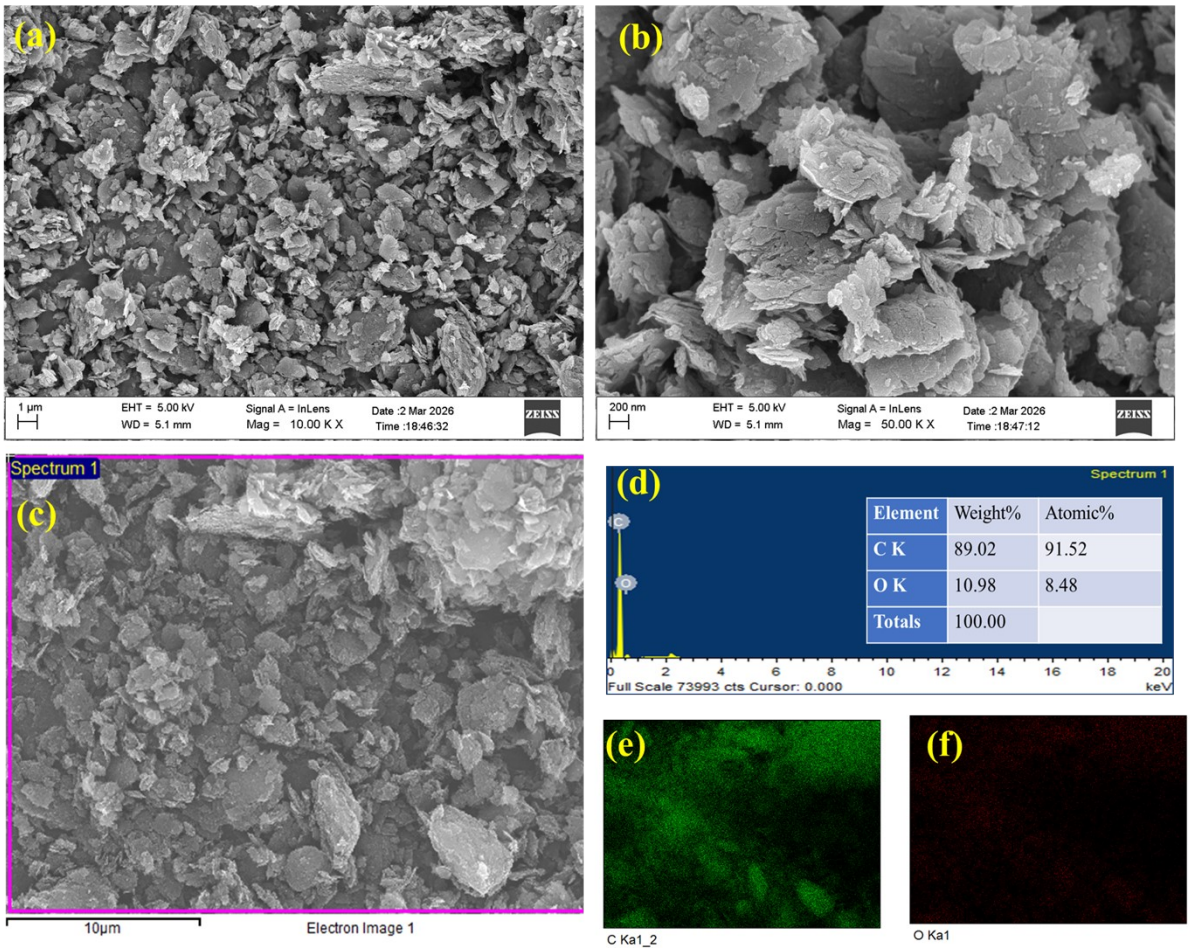

Figure S7 (a) FESEM micrograph for the rGO at a magnification of (a)10 KX and (b) 50 KX. (c) Electronics image of rGO, The EDX spectrum of rGO, (c) FE-SEM micrograph for elemental mapping of rGO, (e) carbon, (f) oxygen.

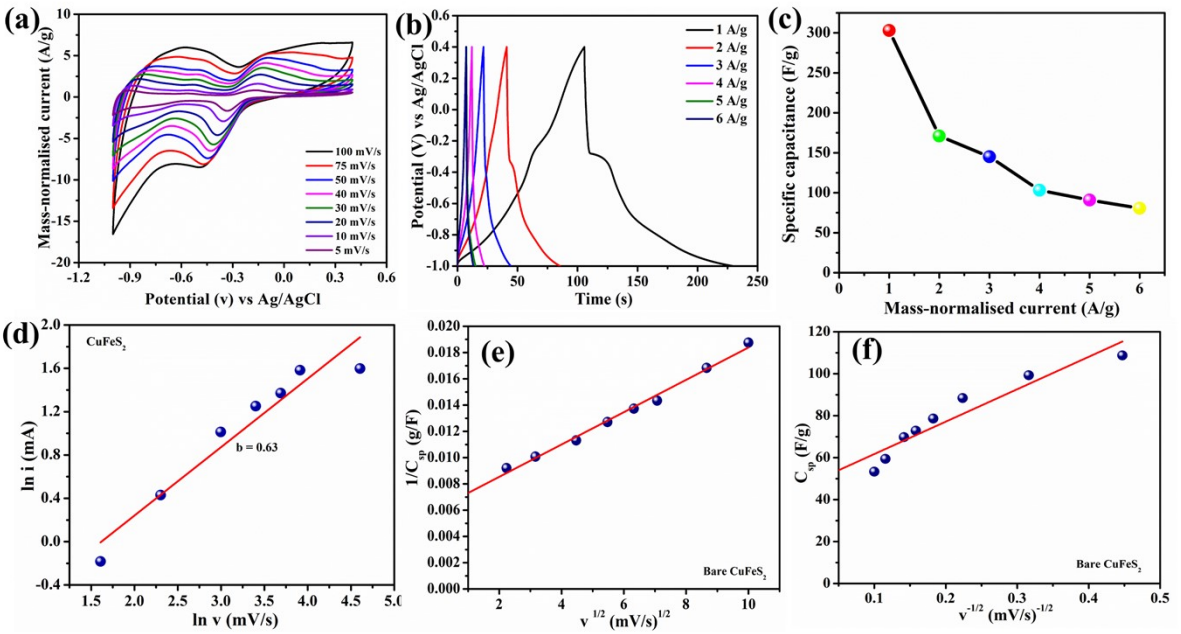

Figure S8 Electrochemical analysis of prepared $CuFeS_2$: **(a)** CV plots of $CuFeS_2$ electrode at various scan rates (i.e., 5 to 100 mV/s). **(b)** CD plots for the $CuFeS_2$ at different applied currents from 1 A/g to 6 A/g, **(c)** effect of different applied mass-normalised current values on the specific capacitance of the $CuFeS_2$. Calculating the b-parameter using the power law equation. This parameter represents the slope of the linear relationship between the ln of the current and the ln of the scan rate in (d) $CuFeS_2$. Trasatti plots for $CuFeS_2$ electrode. (e) shows the relationship between $1/C_{sp}$ and $v_{1/2}$, (f) the relationship between C_{sp} and v.

Table S5 Specific capacitance and specific capacity values for bare $CuFeS_2$.

Sr. no.	Sample	Mass normalised current (A/g)	Specific Capacitance (F/g)	Specific Capacity (C/g)
1.	$CuFeS_2$	1	303.03	424.32
		2	170.94	239.32
		3	144.997	203.00
		4	103.252	144.55
		5	90.925	127.30
		6	80.640	112.90

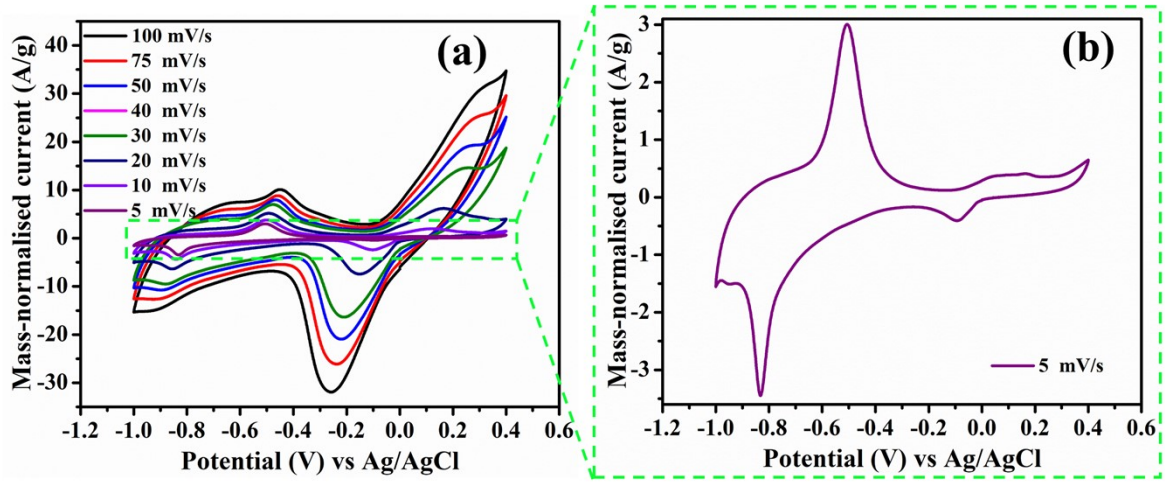

Figure S9 (a) CV plots of $CuFeS_2$@rGO composite electrode at various scan rates (i.e., 5 to 100 mV/s); (b) image displays an enlarged view of 5 mV/s for $CuFeS_2$@rGO.

Table S6 Specific capacitance and specific capacity values for $CuFeS_2$@rGO.

Sr. no.	Sample	Mass normalised current (A/g)	Specific Capacitance (F/g)	Specific Capacity (C/g)
1.	$CuFeS_2$@rGO	1.0	1160.02	1624.03
		1.5	0785.34	1099.48
		2.0	0621.11	869.55
		2.5	0496.03	694.44
		3.0	0466.42	653.00
		3.5	0343.47	480.86
		4.0	0324.41	454.17
		4.5	0243.24	340.54
		5.0	0242.13	339.00

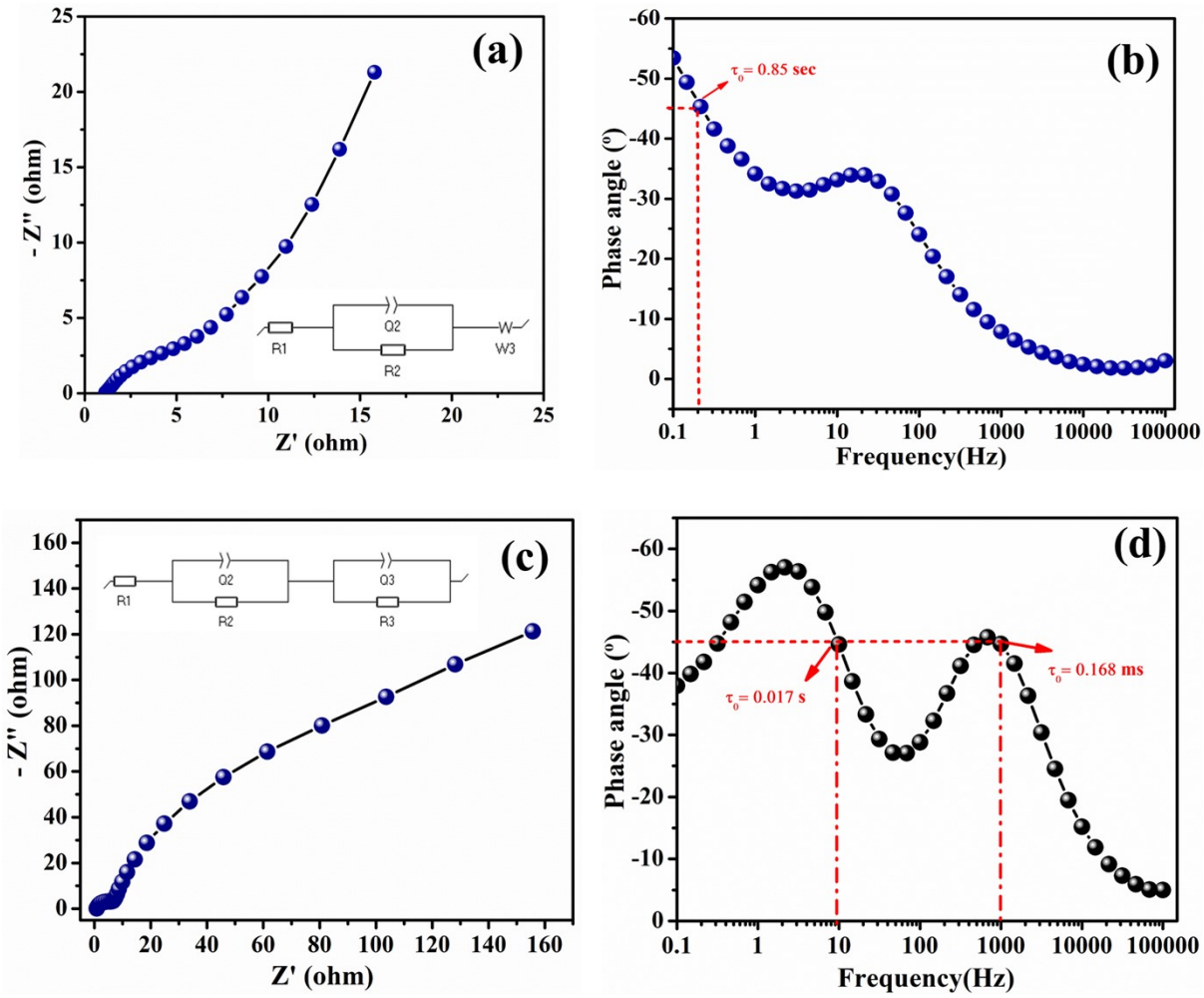

Figure S10 (a) Nyquist plot for bare $CuFeS_2$ electrode, with inset showing the equivalent Randle circuit; (b) Bode plots for bare $CuFeS_2$ electrode with the relaxation time constant; (c) Nyquist plot for $CuFeS_2$@rGO electrode, with inset showing the equivalent Randle circuit; (d) Bode plots for $CuFeS_2$@rGO electrode with the relaxation time constant.

Table S7 EIS fitted data for bare $CuFeS_2$ and $CuFeS_2$@rGO composite.

Sample name	R_1 (solution resistance) (Ω)	R_2 (charge–transfer resistance) (Ω)	C_{dl} ($F.s^{n-1}$)	n_{dl}	τ_0 (s)
$CuFeS_2$	1.05	14.66	13.9×10^{-6}	0.90	0.85
$CuFeS_2$@rGO	0.89	8.2	4.4×10^{-4}	0.89	1.68×10^{-4}
$CuFeS_2$@rGO (bulk)	-	-	5.8×10^{-3}	0.84	0.017

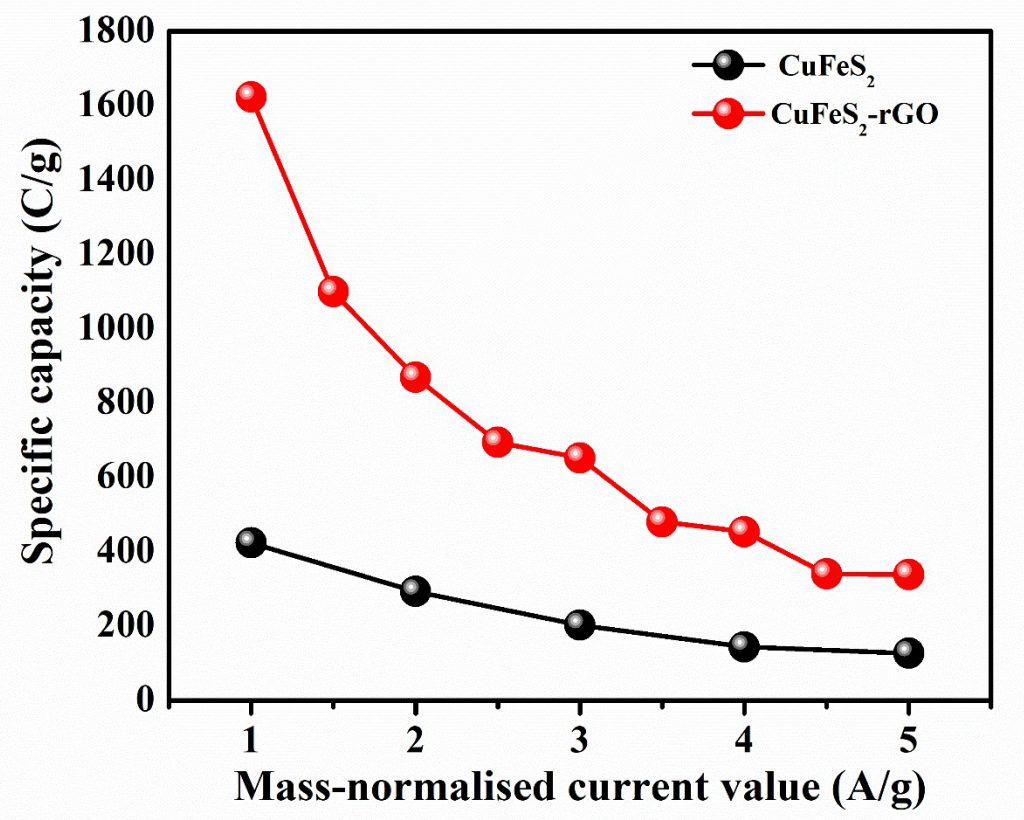

Figure S11 Comparison of Specific capacity for bare $CuFeS_2$ electrode and $CuFeS_2$@rGO composite.

Table S8 EIS fitted data for the $CuFeS_2$@rGO//$CuFeS_2$@rGO composite device.

Sample name	R_1 (solution resistance) (Ω)	R_2 (charge–transfer resistance) (Ω)	C_{dl} ($F.s^{n-1}$)	n_{dl}	W (Warburg element) ($Ω.s^{-1/2}$)	τ_0 (s)
$CuFeS_2$@rGO (SSDs)	1.18	0.74	3.2×10^{-4}	0.93	46.8	0.013

Table S9 Specific capacitance and specific capacity value for the symmetric cell device at different mass-normalised current values.

Sr. no.	Sample	Mass normalised current (A/g)	Specific Capacitance (F/g)	Specific Capacity (C/g)
1.	$CuFeS_2$@rGO//$CuFeS_2$@rGO SSDs	0.5	64.94	90.92
		0.6	42.58	59.61
		0.7	35.77	50.08
		0.8	29.75	41.65
		0.9	24.39	34.15
		1.0	20.96	29.34
		1.5	14.13	19.78
		2.0	9.61	13.45
		2.5	6.64	9.30
		3.0	5.03	7.04

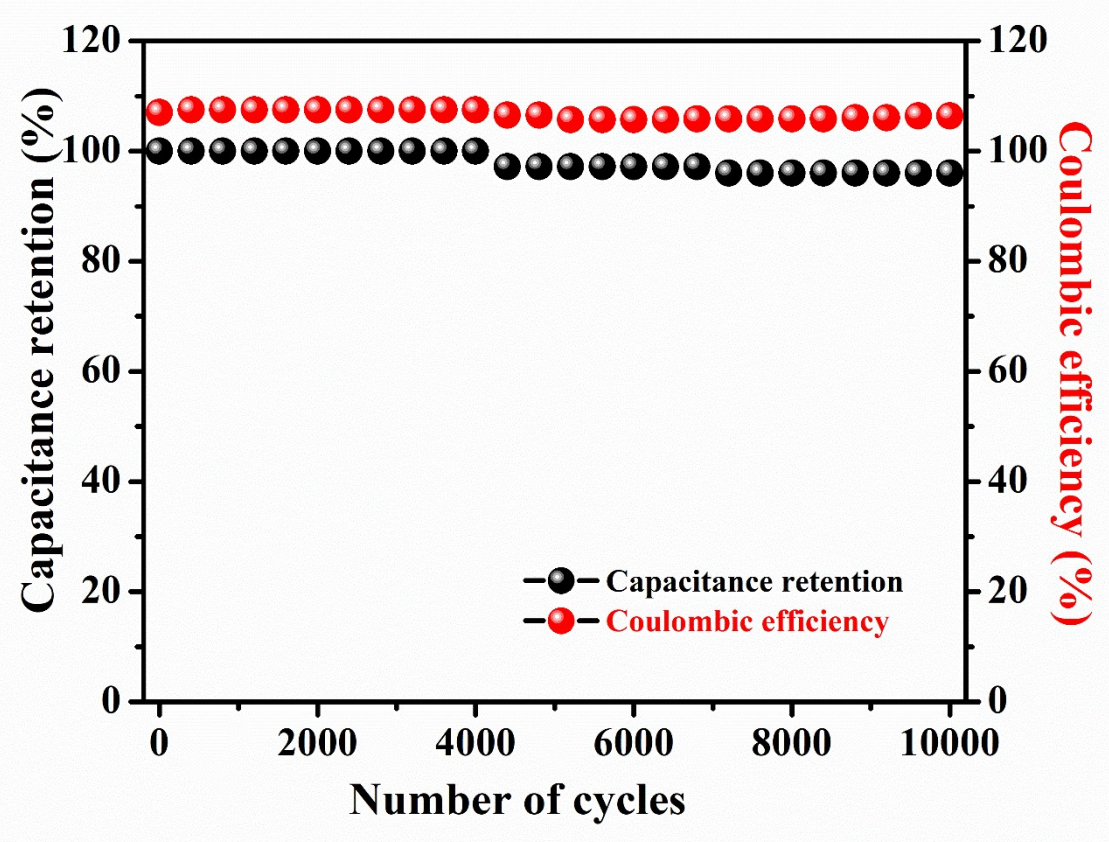

Figure S12 Cyclic stability of the assembled device at the mass-normalised current value of 5 A/g, with the coulombic efficiency.

Table S10 Comparison of supercapacitor performance of three-electrode measurements with published reports

Sr. no.	Electrode material	Method	Electrolyte	Specific capacitance (F/g)	Reference
1	Ni_3S_2/MWCNT	Hydrothermal	2 MKOH	800	S1
2	CoS/rGO	Hydrothermal	6 mol/L KOH	550	S2
3	CoS@rGO	Soak and hydrothermal	2 M KOH	849	S3
4	rGO-CNT	Hummer method	6 M KOH	977	S4
5	Co_3S_4@rGO	Facial two-step method	2 M KOH	675.9	S5
6	RGO/FeS	Hydrothermal	2 M KOH	300	S6
7	$FeNiS_2$@rGO	Hummer method	2 M KOH	1013	S7
8	Fe_3S_4/RGO	Solvothermal method	1 M KOH	560	S8
9	rGO-Fe_3O_4	Hydrothermal	1 M Na_2SO_4	182.2	S9
10	**$CuFeS_2$@rGO**	**Hydrothermal**	**1 M Na_2SO_4**	**1160.02**	**This work**

Table S11 Comparison of supercapacitor performance of assembled symmetric Supercapacitive device (SSD) with published reports.

Sr. no.	Device	Specific capacitance (F/g)	Specific energy density (Wh/kg)	Specific power density (W/kg)	Reference
1	NiS	11.15	0.991	261.11	S10
2	FeS	4.62	2.26	726	S11
3	$AgFeS_2$	331	45	0.261	S12
4	$CuFeS_2$	34.18	4.74	1666	S13
5	Cu_4SnS_4	34.9	2.4	0.291	S14
6	Co_3S_4-rGO	164 mF/cm^2	1.09	750	S15
7	$CuFeS_2$-CC	120	16	1146	S16
8	NiS/MoS_2@N-rGO	1028	35.69	601.8	S17
9	**$CuFeS_2$@rGO**	**64.94**	**17.67**	**3141.4**	**This work**

Reference:

(S1) Dai, C.-S.; Chien, P.-Y.; Lin, J.-Y.; Chou, S.-W.; Wu, W.-K.; Li, P.-H.; Wu, K.-Y.; Lin, T.-W. Hierarchically Structured Ni3S2/Carbon Nanotube Composites as High

Performance Cathode Materials for Asymmetric Supercapacitors. *ACS Appl. Mater. Interfaces* **2013**, *5* (22), 12168–12174. https://doi.org/10.1021/am404196s.

(S2) Xu, L.; Lu, Y. One-Step Synthesis of a Cobalt Sulfide/Reduced Graphene Oxide Composite Used as an Electrode Material for Supercapacitors. **2015**. https://doi.org/10.1039/C5RA11711A.

(S3) Song, X.; Tan, L.; Wang, X.; Zhu, L.; Yi, X.; Dong, Q. Synthesis of CoS@rGO Composites with Excellent Electrochemical Performance for Supercapacitors. *Journal of Electroanalytical Chemistry* **2017**, *794*, 132–138. https://doi.org/10.1016/j.jelechem.2017.04.014.

(S4) Mohammadi, A.; Arsalani, N.; Tabrizi, A. G.; Moosavifard, S. E.; Naqshbandi, Z.; Ghadimi, L. S. Engineering rGO-CNT Wrapped Co3S4 Nanocomposites for High-Performance Asymmetric Supercapacitors. *Chemical Engineering Journal* **2018**, *334*, 66–80. https://doi.org/10.1016/j.cej.2017.10.029.

(S5) Wang, Q.; Jiao, L.; Du, H.; Si, Y.; Wang, Y.; Yuan, H. Co3S4 Hollow Nanospheres Grown on Graphene as Advanced Electrode Materials for Supercapacitors. *J. Mater. Chem.* **2012**, *22* (40), 21387–21391. https://doi.org/10.1039/C2JM34714H.

(S6) Zhao, C.; Shao, X.; Zhu, Z.; Zhao, C.; Qian, X. One-Pot Hydrothermal Synthesis of RGO/FeS Composite on Fe Foil for High Performance Supercapacitors. *Electrochimica Acta* **2017**, *246*, 497–506. https://doi.org/10.1016/j.electacta.2017.06.090.

(S7) Miah, M.; Hota, P.; Mondal, T. K.; Chen, R.; Saha, S. K. Mixed Metal Sulfides (FeNiS2) Nanosheets Decorated Reduced Graphene Oxide for Efficient Electrode Materials for Supercapacitors. *Journal of Alloys and Compounds* **2023**, *933*, 167648. https://doi.org/10.1016/j.jallcom.2022.167648.

(S8) Karuppasamy, M.; Muthu, D.; Haldorai, Y.; Rajendra Kumar, R. T. Solvothermal Synthesis of Fe3S4@graphene Composite Electrode Materials for Energy Storage. *Carbon Lett.* **2020**, *30* (6), 667–673. https://doi.org/10.1007/s42823-020-00139-9.

(S9) Wang, H.; Xu, X.; Wang, C.; Neville, A.; Hua, Y. Fundamental Insight into the Degradation Mechanism of an rGO-Fe3O4 Supercapacitor and Improving Its Capacity Behavior via Adding an Electrolyte Additive. *Energy Fuels* **2021**, *35* (9), 8406–8416. https://doi.org/10.1021/acs.energyfuels.1c00653.

(S11) Karade, S. S.; Dwivedi, P.; Majumder, S.; Pandit, B.; Sankapal, B. R. First Report on a FeS-Based 2 V Operating Flexible Solid-State Symmetric Supercapacitor Device. *Sustain. Energy Fuels* **2017**, *1* (6), 1366–1375. https://doi.org/10.1039/C7SE00165G.

(S12) Abdullah, M.; Alahmari, S. D.; Aman, S.; Ejaz, S. R.; Haleem, Y. A.; Gouadria, S.; Al-Sehemi, A. G.; Henaish, A. M. A.; Ahmad, Z.; Farid, H. M. T. Facile Fabrication of AgFeS2 Nanostructure via Hydrothermal Route for Supercapacitor Application. *J. Energy Storage* **2024**, *77*, 109875. https://doi.org/10.1016/j.est.2023.109875.

(S13) Sahoo, S.; Pazhamalai, P.; Mariappan, V. K.; Veerasubramani, G. K.; Kim, N.-J.; Kim, S.-J. Hydrothermally Synthesized Chalcopyrite Platelets as an Electrode Material for Symmetric Supercapacitors. *Inorg. Chem. Front.* **2020**, *7* (7), 1492–1502. https://doi.org/10.1039/C9QI01335K.

(S14) Lokhande, A. C.; Patil, A.; Shelke, A.; Babar, P. T.; Gang, M. G.; Lokhande, V. C.; Dhawale, D. S.; Lokhande, C. D.; Kim, J. H. Binder-Free Novel Cu4SnS4 Electrode for High-Performance Supercapacitors. *Electrochimica Acta* **2018**, *284*, 80–88. https://doi.org/10.1016/j.electacta.2018.07.170.

(S15) Patil, S. J.; Kim, J. H.; Lee, D. W. Graphene-Nanosheet Wrapped Cobalt Sulphide as a Binder Free Hybrid Electrode for Asymmetric Solid-State Supercapacitor. *J. Power Sources* **2017**, *342*, 652–665. https://doi.org/10.1016/j.jpowsour.2016.12.096.

(S16) Rupa Ranjani, P.; Anjana, P. M.; Rakhi, R. B. Solvothermal Synthesis of CuFeS2 Nanoflakes as a Promising Electrode Material for Supercapacitors. *J. Energy Storage* **2021**, *33*, 102063. https://doi.org/10.1016/j.est.2020.102063.

(S17) Xu, X.; Zhong, W.; Zhang, X.; Dou, J.; Xiong, Z.; Sun, Y.; Wang, T.; Du, Y. Flexible Symmetric Supercapacitor with Ultrahigh Energy Density Based on NiS/MoS2@N-rGO Hybrids Electrode. *J. Colloid Interface Sci.* **2019**, *543*, 147–155. https://doi.org/10.1016/j.jcis.2019.02.054.

(S18) Barkat, L.; Hamdadou, N.; Morsli, M.; Khelil, A.; Bernède, J. C. Growth and Characterization of CuFeS2 Thin Films. *J. Cryst. Growth* **2006**, *297* (2), 426–431. https://doi.org/10.1016/j.jcrysgro.2006.10.105.

(S19) Fatimah, S.; Ragadhita, R.; Husaeni, D. F. A.; Nandiyanto, A. B. D. How to Calculate Crystallite Size from X-Ray Diffraction (XRD) Using Scherrer Method. *ASEAN J. Sci. Eng.* **2022**, *2* (1), 65–76. https://doi.org/10.17509/ajse.v2i1.37647.